nature chemistry

SUPPLEMENTARY INFORMATION

https://doi.org/10.1038/s41557-018-0105-9

In the format provided by the authors and unedited.

Direct knock-on of desolvated ions governs strict ion selectivity in K^+ channels

Wojciech Kopec[1], David A. Köpfer[1], Owen N. Vickery[2,3], Anna S. Bondarenko[4], Thomas L. C. Jansen[4], Bert L. de Groot[1*] and Ulrich Zachariae[2,3*]

[1]Biomolecular Dynamics Group, Max Planck Institute for Biophysical Chemistry, Göttingen, Germany. [2]Computational Biology, School of Life Sciences, University of Dundee, Dundee, UK. [3]Physics, School of Science and Engineering, University of Dundee, Dundee, UK. [4]University of Groningen, Zernike Institute for Advanced Materials, Groningen, The Netherlands. *e-mail: bgroot@gwdg.de; u.zachariae@dundee.ac.uk

SUPPLEMENTARY INFORMATION

Direct knock-on of desolvated ions governs strict ion selectivity in K^+ channels

Authors: Wojciech Kopec, David A. Köpfer, Owen N. Vickery, Anna S. Bondarenko, Thomas L.C. Jansen, Bert L. de Groot, Ulrich Zachariae

INDEX

1. Materials and Methods

1.1 Molecular Dynamics simulations - computational electrophysiology

We studied spontaneous ion permeation through KcsA and MthK channels, in pure and mixed K^+/Na^+ solutions, driven by the transmembrane voltage induced by charge imbalances as implemented in the CompEL (computational electrophysiology) method in GROMACS[1,2].

System preparation and simulation protocol

For open-state KcsA, we used the x-ray structure (PDB id: 3f5w[3]), with the selectivity filter in the conductive configuration (PDB id: 1k4c[4]), as reported in our previous simulations[5]. For MthK, we used the open state channel crystal structure (PDB id: 3ldc[6]).

In each system, the titratable groups of the protein were protonated according to their standard protonation states at pH 7 (in KcsA E71 was additionally protonated[7]) and inserted into a patch of POPC lipids surrounded by water molecules, K^+, Na^+ and Cl^- ions (see Table S1). After a multi-step equilibration phase, with a gradual release of position restraints on the protein heavy atoms, systems were simulated without any restraints for 20 ns, and then duplicated along the z-axis, perpendicular to the membrane surface, to construct dual bilayer systems typical for CompEL. All simulations were carried out with GROMACS 5.0 or 5.1[8-11], using the CompEL scheme, with an ionic imbalance between the compartments of $2e^-$, yielding a transmembrane voltage of ~220mV. A list of all simulations is shown in Supplementary Tables 1-9.

Simulation details

We used the amber99sb force field[12] in combination with a range of different water models (SPC/E[13], TIP3P[14] and TIP4PEw[15] together with the ion parameters developed by Joung & Cheatham, adapted for each water model[16] in case of KcsA (see Fig. 1 in the main text and Supplementary Fig. 1). For MthK simulations we used the TIP3P variant. Lipids were modeled using Berger parameters[17] adapted for amber99sb[18,19]. Aliphatic hydrogen atoms were treated using the virtual sites approach[20,21] and all bonds were constrained using LINCS[22], allowing for an integration time step of 4fs. Neighbour lists were updated with the Verlet list scheme[23]. The

van-der-Waals interactions were cut off at 1.0 nm and we applied the dispersion correction for energy and pressure. The Particle Mesh Ewald (PME) method[24] was used for long-range electrostatic interactions, with a 1.0 nm real space cutoff. The simulated systems were kept at a temperature of 320K and a pressure of 1bar, using the v-rescale thermostat[25], and a semi-isotropic Berendsen barostat[26], respectively, to maintain an NPT ensemble. Control simulations using a 2 fs time step showed that the usage of virtual sites and a larger time step do not affect the observed ion permeation mechanism or recorded ion currents.

In simulations of KcsA, a network of hydrogen bonds were restrained to stabilize the secondary structure of the truncated termini of the S6 helices and distance restraints were used to keep the channel in an open conformation. Additionally, F103 residues were distance restrained in order to prevent dehydration of the pore cavity.

1.2 Molecular Dynamics simulations – applied electric field

For studies of ion permeation in Kv1.2 W362Y, NaK2K and non-selective NaK2CNG-N channels, we used a single membrane approach, with an applied electric field along the z-axis (parallel to the SF axis).

System preparation and simulation protocol

For the open-state Kv1.2 W362Y we used the pore domain from the 'paddle-chimera' Kv1.2-Kv2.1 structure (PDB id: 2r9r)[27]. In this structure, the channel remains in an open, conductive conformation under positive voltages[28]. The titratable groups of the protein were protonated according to their standard protonation states at pH 7. We replaced tryptophan residues at the position 362 to tyrosines in all four subunits. Experimentally, this mutation yields a channel with comparable conductive and selective properties to wild-type rat Kv1.6[29], while in simulations we found that W to Y substitution stabilizes the selectivity filter due to the stabilization of D375 in its crystallographic position behind the selectivity filter. The protein was embedded in a POPC membrane and surrounded with water molecules and K^+ and Cl^- ions, corresponding to a salt concentration of ~900 mM, using the CHARMM-GUI webserver[30-33]. The initial, multi-step equilibration was conducted using scripts provided by CHARMM-GUI[34]. Subsequently, the

system was equilibrated for 50 ns before the production runs, that were performed in both amber99sb*-ILDN[35] (Fig. 2 in the main text) and CHARMM36 force fields (Supplementary Fig. 2). Simulations of wild type Kv1.2 (Kv1.2 WT) were performed with the CHARMM36 force field with and without position restraints on D375 (Supplementary Fig. 14).

For the open-state NaK2K and non-selective NaK2CNG-N we used the available high-resolution open structures (PDB id: 3ouf and PDB id: 3k06)[36,37]. All the preparation steps were carried out in the same manner as for Kv1.2. We introduced the F92A mutation to increase the currents, as in experiments[38]. The final systems were simulated with both amber99sb (Fig. 2 in the main text) and CHARMM36 (Supplementary Fig. 2) force fields in case of NaK2K, while amber99sb was used for NaK2CNG-N.

After the equilibration, an external electric field was applied along the z-axis (parallel to the SF axis), to establish a transmembrane voltage of ~280 mV. The transmembrane voltage V was calculated following Roux[39,40]:

$$V = E \cdot L_z \quad (1)$$

where E is the applied electric field (typically between 0.033 and 0.037 V/nm) and L_z is the length of the box along the z-axis (fluctuating between 7.6 and 9.4 nm in our simulations).

Simulation details

For simulations with the amber99sb force field, all parameters were identical to these used in simulations of KcsA and MthK. For Kv1.2 W362Y we used amber99sb*-ILDN[35,41] that further stabilizes D375. All remaining parameters and input options were identical to these used in other simulations with amber99sb.

For simulations with the CHARMM36 force field, used the latest version of the CHARMM36 force field[42,43], termed CHARMM36m[44], downloaded from http://mackerell.umaryland.edu/charmm_ff.shtml (accessed in January 2017), which contains all necessary parameters for the protein, lipids and ions. Water was modeled using the CHARMM version of TIP3P, with LJ interactions placed on hydrogens. For ions, we used standard CHARMM parameters[45]. Note that the same force field was used previously in extended simulations of Kv1.2[46]. All hydrogen-containing bonds were constrained using LINCS, and a time step of 2 fs was used. Van der Waals interactions were force-switched off from 0.8 to 1.2

nm. Long-range electrostatic interactions were treated with PME, with a 1.2 nm real space cutoff. The simulated systems were kept at a temperature of 320K and a pressure of 1 bar, using a Nosé-Hoover thermostat[47,48] and a Parrinello-Rahman barostat[49], respectively.

In the set of restrained simulations of Kv1.2 WT, the carbon atoms from side chains of residues D375 were position-restrained with a force constant of 500 kJ/mol/nm^2 to their crystallographic positions.

1.3 Spectral 2D IR calculations

Recently, the 'direct Coulomb knock-on' mechanism was challenged by the interpretation of experimental 2D IR spectroscopic measurements via atomistic simulation combined with theoretical spectral calculations[50]. We performed similar calculations using the SF occupancy states observed in our computational electrophysiology simulations, and compared them with the experimental spectrum.

System preparation and calculation protocol

In our 2D IR calculations, we used a single KcsA channel embedded in a POPC membrane, similar to the system reported in Kratochvil et al.[50]. The starting structure was initially extensively simulated under an applied voltage (~280 mV) to ensure that the channel remains in the conductive conformation. Like in our computational electrophysiology simulations, all ion permeation events occurred through the 'direct Coulomb knock-on' mechanism in these simulations, i.e. through intimate interactions between two or more ions. Next, a number of specific occupancy states of the SF, corresponding to ion-conductive configurations, were selected (see Supplementary Table 10), and further equilibrated at 0 mV for 10 ns per state, to mimic the conditions of the IR experiments. To ensure that a given occupancy state does not change during the equilibration, flat-bottomed position restrains were applied on K^+ ions in the SF (sites S1 to S4). Since the KWKW and WKWK occupancy states, characteristic for the 'soft knock-on' mechanism[50,51], were never observed during ion permeation in our simulations, they were generated manually and extensively equilibrated (1200 ns per occupancy state) at 0 mV. Again, only K^+ ions in the SF were restrained in these simulations. Since in these water-containing states a single backbone carbonyl group of Val76 sometimes shows flips away from

the main axis of the SF as reported earlier[50], we considered these states separately (see Supplementary Table 10). To ensure that spontaneous flipped–nonflipped transitions do not affect the final spectrum for a given state, a set of simulations (for 4 states: KWKW and WKWK, both with flipped and nonflipped Val76) was repeated with position restraints on carbonyl oxygen atoms of Val76. The resulting spectra were very similar to these obtained without such restraints.

Subsequently, a number of snapshots (at least 9 per single occupancy state) were randomly selected from the last 2 ns of equilibration. Each snapshot was then used as a starting point for a simulation of 1 ns length, during which the positions of atoms were saved every 20 fs. These trajectories were then used for spectral calculations. All presented spectra for individual occupancy states (Supplementary Fig. 5) are averages over at least 5 independent simulations of 1 ns.

The spectral calculations were performed by first extracting the amide I Hamiltonian, transition dipoles and site frequencies from the 1 ns trajectories. Next, the amide units corresponding to those labeled in the experiment[50], were selected and their frequencies were shifted by -66 cm^{-1} to account for the isotope label. The anharmonicity was kept constant at 14 cm^{-1}. Finally, 1D and 2D IR spectra were calculated with the numerical integration of the Schrödinger equation method (NISE)[52,53]. In this method, the excitations are localized on the amide I modes, and the integration is performed in small time steps, during which the Hamiltonian is considered constant. This allows calculating the linear response function as well as the third-order response functions. The linear 1D spectrum is then obtained by a Fourier transform of the linear response function, while the 2D spectrum is obtained with a two-dimensional Fourier transform with respect to the coherence times.

Spectral calculation details

The amide I Hamiltonian, frequencies and couplings were calculated using the AmideIMaps program, developed as an add-on to GROMACS 4.6.3. The Skinner electrostatic map[54] was used, which relates the electric field generated by the force field point charges on each atom of the amide I unit with the site frequency and the transition dipole. Its good performance in combination with the Amber force field has recently been assessed[55,56].The cut-off for calculating electric fields/gradients was 2.0 nm. The short-range couplings and frequency shifts

were calculated using the nearest neighbor coupling model[57]. The long-range couplings were calculated using the transition dipole coupling (TDC) model[58]. 1D and 2D IR spectra, together with the Fourier transformations, were calculated using the NISE3 code[53]. In all simulations the waiting time between the pump and probe was set to zero. The coherence times were varied from 0 to 5 ps in 20 fs steps. The response functions were Fourier transformed for the coherence times leading to the two frequency axes. The spectral windows for calculations were set to the range 1400-1800 cm^{-1}.

Data analysis

All presented spectra are for the ZZZZ parallel combination. First, 2D IR spectra were plotted for each trajectory and each occupancy state. They were carefully assessed for any possible artifacts, which could for instance arise due to transient interactions between bound K^+ and aqueous Cl^- ions, water influx behind the SF, etc. Then, the spectra were averaged, resulting in one representative spectrum per occupancy state (Supplementary Fig. 5). Finally, spectra for different occupancies were linearly combined, with varying weights (Fig. 3 in the main text and Supplementary Fig. 4). Note that this is the same approach as used for the states characteristic for the 'soft knock-on' mechanism in Kratochvil et al.[50]. Here, the same averaging procedure was used in all cases.

The frequencies were shifted by an empirical correction of +13 cm^{-1} [55].The optimal weights and the resulting theoretical spectrum for states characteristic for the 'direct knock-on' mechanism are shown in the main manuscript (Fig. 3). A similar plot for the 'soft knock-on' mechanism is shown in Supplementary Fig. 4. Plotting and averaging was performed using in-house written Python scripts. The nodal line slopes were calculated by identifying ω_{probe} with the highest bleach peak intensity for each ω_{pump}, and fitting the pairs to a straight line. Values within the [max(ω_{probe}) - 10, max(ω_{probe}) + 10] range were considered for the slope calculation. The slope is then given by a number between 0 and 1, where a value close to one means that there is a high degree of inhomogeneity, while values near zero indicate a homogenous system. Slope calculations were performed using custom Perl scripts.

1.4 Molecular Dynamics simulations - free energy calculations

We performed free energy calculations for individual binding sites in the SF of KcsA to assess their thermodynamic preference for either K^+ or Na^+ ions. By definition, the thermodynamic selectivity for a given site is given by:

$$\Delta\Delta G_{K,Na} = \Delta G^{site}_{K,Na} - \Delta G^{water}_{K,Na} \quad (2)$$

where $\Delta G^{water}_{K,Na}$ is the free energy difference for 'alchemically' transforming K^+ to Na^+ in bulk water (which is equal to -74.8 kJ/mol[59,60]), whereas $\Delta G^{site}_{K,Na}$ is the free energy difference for the same transition at the binding site. Therefore, a positive value of $\Delta\Delta G_{K,Na}$ implies a K^+ selective site, and conversely, a negative value implies a Na^+ selective site.

System preparation and simulation protocol

We investigated the thermodynamic selectivity at the specific binding sites in the SF, for the occupancy states most frequently visited during ion permeation. Consequently, we focused on KK0K and 0KKK occupancies (see Supplementary Fig. 8). Three snapshots per occupancy pattern were selected from the computational electrophysiology simulations, transformed back to a single membrane setup, and further equilibrated for 40 ns at 0 mV. The final snapshots from these simulations were then used for K^+ to Na^+ alchemical free energy calculations to obtain $\Delta G^{site}_{K,Na}$ for each occupied site. The alchemically transformed ions were held in place along the z-axis (parallel to the SF axis) at their preferential binding sites located at the center of mass of eight neighboring carbonyl oxygen atoms (canonical ion binding sites), with spherical flat-bottomed restraints.

To assess the existence and selectivity of potential Na^+ binding sites in the SF, as previously suggested[61,62], we introduced a single Na^+ ion instead of a K^+ ion at each site for both starting occupancies, ultimately resulting in the following occupancies: KNaK, NaKK, KKNa (see Supplementary Fig. 8). After 40 ns of equilibration, the introduced Na^+ ions moved to their preferred binding sites, in plane with four SF carbonyl oxygen atoms. Subsequently, three snapshots per state were used for Na^+ to K^+ alchemical free energy calculations. In this case, the alchemically transformed Na^+ ion was held at its preferred in-plane binding site at the center of mass of four carbonyl oxygen atoms with identical flat-bottomed restraints (the only exception

was one of the KNaK occupancy states, where in one case the Na^+ ion preferred to occupy the canonical S3 binding site; therefore it was kept there with identical restraints as those used for the K^+ ions).

The free energy difference between K^+ and Na^+ in bulk water was obtained by performing identical alchemical free energy calculations in a cubic box of ~2100 water molecules and one ion, with the same parameters as in the K^+ channel simulations. The value we obtained (-74.8 kJ/mol) perfectly matches the difference in absolute hydration free energies between K^+ and Na^+ for the force field used[16] as well as the experimental data[59,60]. Control simulations with a 2 fs time step showed that the usage of a larger time step (4 fs) does not affect the calculated free energies.

Simulation details

All the force field parameters and input options were identical to those used for the computational electrophysiology simulations (amber99sb with SPC/E water variant). The temperature was set to 298 K. To calculate the free energy differences between K^+ and Na^+, we employed the free energy code in GROMACS, using a linear coupling scheme with 21 lambda windows, covering the lambda space from 0 to 1. Each of these windows was energy minimized by 5000 steps of steepest descent and simulated twice, each for 8 ns, resulting in a total simulation time of ~12 μs (12 states, 3 snapshots per state, 2 copies per snapshot, 21 windows, 8 ns per window). The strength of the restraining potential was selected to be 10^5 kJ/mol/nm^2 in all cases, after extensive tests, which ensured that the restrained ion remained in its dedicated site during the alchemical transition (within root mean square fluctuations of ~0.1Å in the Z direction, for both Na^+ and K^+ ions).

Data analysis

The free energy differences, $\Delta\Delta G_{K,Na}$, were calculated using the Multistate Bennett Acceptance Ratio (MBAR) method[63] as implemented in the 'alchemical analysis' software[64]. Various equilibration times ranging from 4 to 7 ns were considered, ensuring that the final number of uncorrelated statistical samples used to evaluate the free energy difference remained above 50 per each lambda window (typically the number of uncorrelated samples was well above 1000). The values reported (Supplementary Table 11) are averages over 6 simulation sets (3 snapshots,

each simulated twice) per site, with uncertainties expressed as root mean square deviations (standard deviations).

2. Supplementary Text

2.1 KcsA simulations

In addition to simulations presented in the main text, we performed additional simulations with the same protein force field (amber99sb) and different water and ion models (TIP3P and TIP4PEw, Supplementary Fig. 1). Both K^+ and Na^+ currents, and the effect of Na^+ ions on the K^+ current, show the same behavior, irrespective of the used force field.

2.2 MthK simulations under a concentration gradient

To test the selectivity of the MthK channel under a concentration gradient rather than a transmembrane voltage, we performed additional simulations using the computational electrophysiology setup, keeping a constant concentration (1 M) of KCl in one compartment, and the same concentration of NaCl in the other one (Supplementary Fig. 10). We observe K^+ current in the outward (physiological) direction and no inward Na^+ current, confirming ion selectivity of potassium channels also under these conditions.

2.3 Kv1.2 WT simulations

In our simulations of Kv1.2 WT, where ion permeation is driven by a constant applied transmembrane voltage of ~280 mV, we observe small K^+ currents (Supplementary Fig. 14) and significant ion-water co-permeation (water/ion ratio >0.4), in agreement with previous simulations of Kv1.2[46]. This different mechanism of ion permeation is a consequence of a different conformation of the SF, where side chains of D375 residues pointing toward the extracellular space, resulting in overall SF instability. Accordingly, the ion selectivity is reduced in these states (Supplementary Fig. 14). In contrast, in our simulations with restraints applied on D375 side chains to maintain them in their crystallographic conformation, we observe large, 'direct knock-on' dominated K^+ currents, with a reduced level of water co-permeation, similar to the Kv1.2 W362Y simulations reported in the main text (Fig 2).

2.4 The relationship between ion dehydration and cation binding to the SF

Our combined findings from the free energy calculations and individual permeation data are consistent with Eisenman's theory of 'field strength'[65,66], which suggested that low and mid-field ligands, such as the carbonyl oxygen atoms in K^+ channels, prefer larger cations, and the

difference in hydration free energy between cations dictates the overall preference of the channel. This theory predates any structural and dynamic information on ion channels. Experimentally, the thermodynamic properties of ion binding to the SF have recently been established for a wide range of mono- and divalent cations by isothermal titration calorimetry (ITC)[67]. Whereas K^+, Rb^+ and Cs^+ ions bind to, and permeate the SF of the KcsA channel, Ba^{2+} ions bind but subsequently block the SF. Li^+, Na^+, Mg^{2+} and Ca^{2+} ions show no binding affinity to the SF in ITC measurements. These observations have been attributed to the size of the ions, as ions of similar and slightly larger radius than K^+ (Rb^+, Cs^+, Ba^{2+}) bind, while smaller ions (Li^+, Na^+, Mg^{2+}, Ca^{2+}) interact only weakly with the SF, but they are also consistent with the trends in their different free energy of dehydration[59,68,69]. In the case of the monovalent ions for instance, Li^+ and Na^+ exhibit much higher dehydration energies than K^+, Rb^+ or Cs^+[59,68,69]. Amongst divalent cations, Ba^{2+} displays by far the lowest dehydration free energy, and therefore can enter the SF, but subsequently its double charge leads to longer retention in the SF and thus filter block[70-72].

3. Supplementary Figures

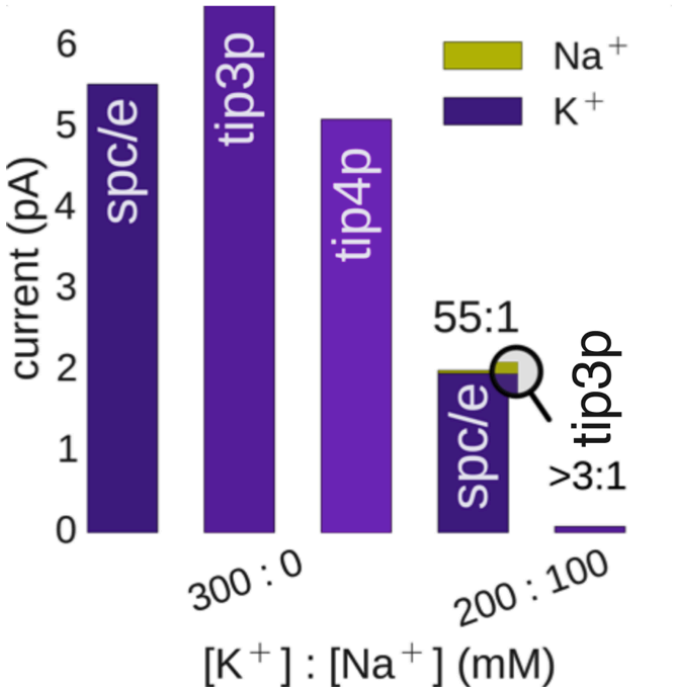

Supplementary Figure 1. Currents in KcsA with different water and ion models. Both K^+ and Na^+ currents, as well as the effect of Na^+ on K^+ currents are similar in each case, independent of the water model.

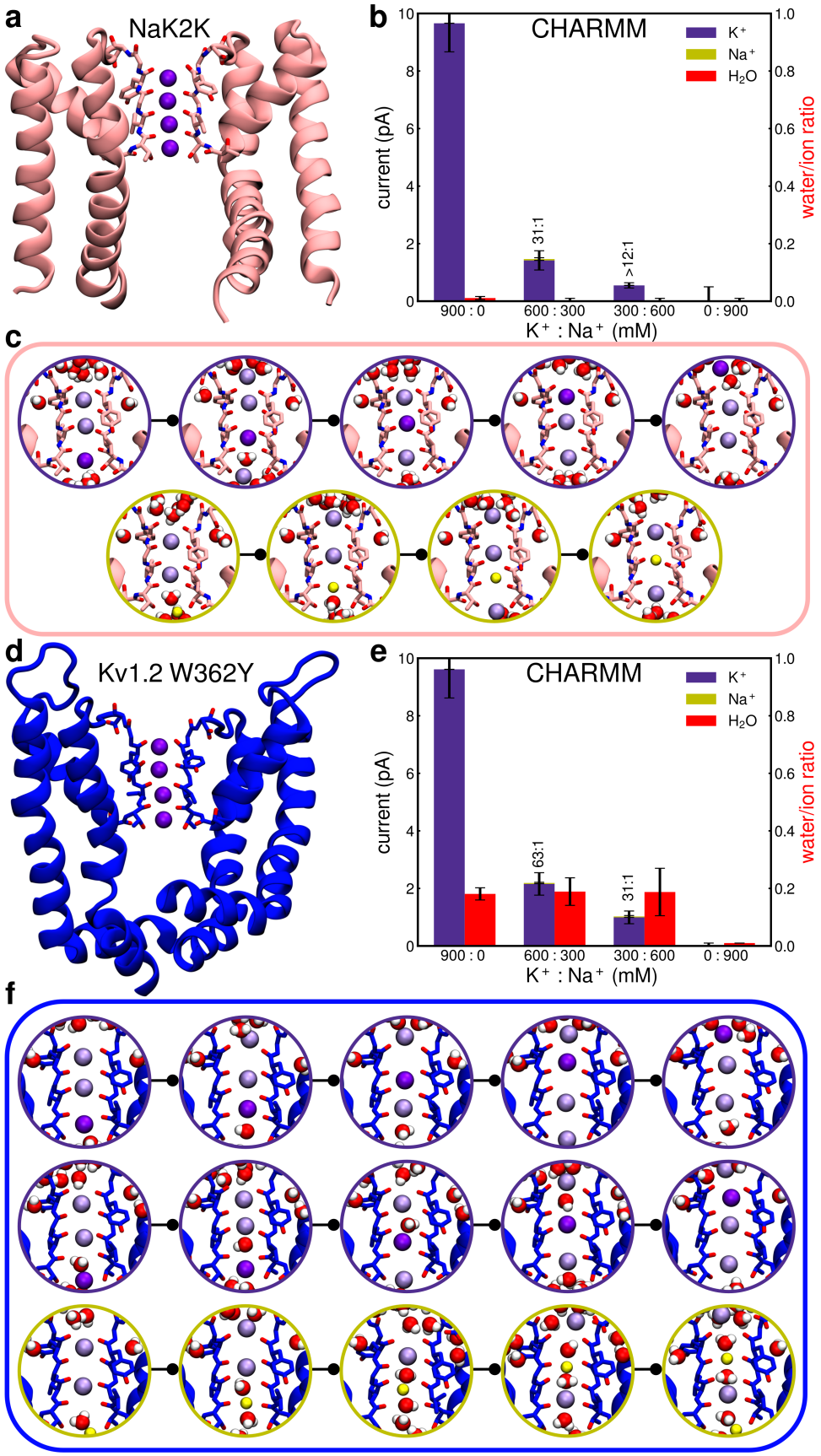
a
NaK2K
b
CHARMM
K+
Na+
H2O
current (pA)
water/ion ratio
31:1
>12:1
900 : 0
600 : 300
300 : 600
0 : 900
K+ : Na+ (mM)
c
d
Kv1.2 W362Y
e
CHARMM
K+
Na+
H2O
current (pA)
water/ion ratio
63:1
31:1
900 : 0
600 : 300
300 : 600
0 : 900
K+ : Na+ (mM)
f

Supplementary Figure 2. Control simulations on NaK2K (a-c) and Kv1.2 W362Y (d-f) performed with the CHARMM force field. The structures of NaK2K **(a)** and Kv1.2 W362Y **(d)** are shown. **(b, e)** Ion currents and water/ion permeation ratios at a voltage of ~280 mV in pure solutions of K^+ or Na^+ as well as in mixed solutions. For NaK2K, the results obtained with CHARMM are very similar to those obtained with amber99sb (Fig. 2 in the main text). NaK2K does not allow water molecules to pass and is K^+ selective, although we see rare events of a Na^+ ion passing the SF **(c)**. In simulations of Kv1.2 W362Y with CHARMM we observe an increased water/ion permeation ratio (up to ~0.2), resulting from water molecules occasionally traversing the SF, although the vast majority of ion permeation events follow the direct knock-on mechanism **(f)**. This allows the channel to maintain a KcsA-like level of ion selectivity **(e)**. The colour code for ions and water in the structure snapshots is the same as in Figs. 1 and 2 of the main text.

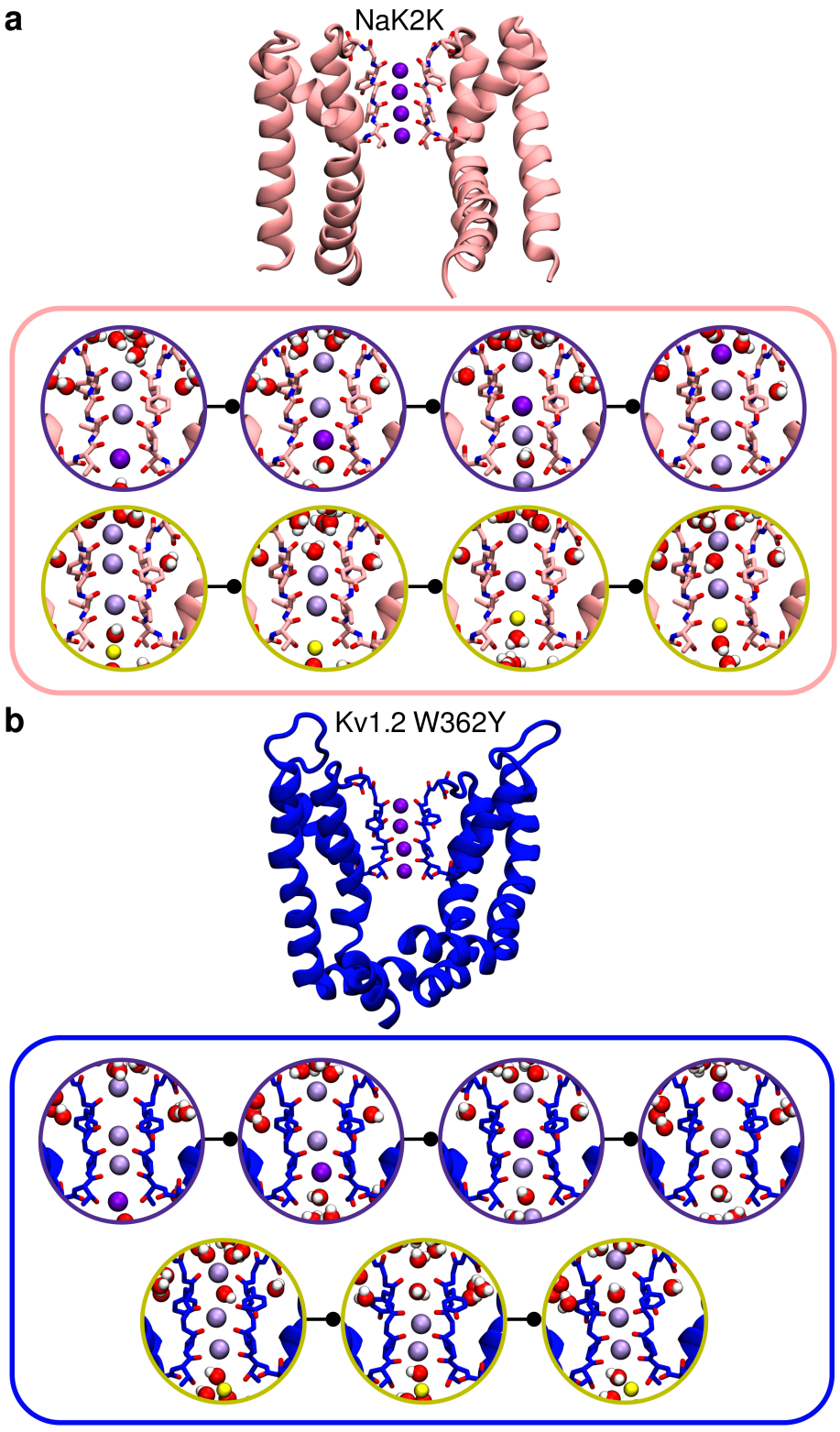
a
NaK2K
b
Kv1.2 W362Y

Supplementary Figure 3. Simulation snapshots showing ion permeation in NaK2K (a) and Kv1.2 W362Y (b) simulations performed with the amber force field. The colour code for ions and water is the same as in Figs. 1 and 2 of the main text.

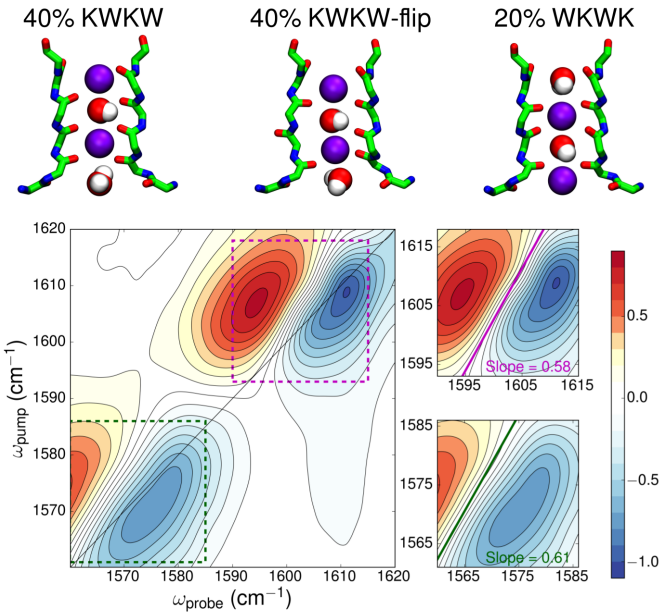

Supplementary Figure 4. Calculated 2D IR spectrum for states characteristic for the 'soft knock-on' mechanism. The weights used to generate the final spectrum are shown above the schematic representation of each state.

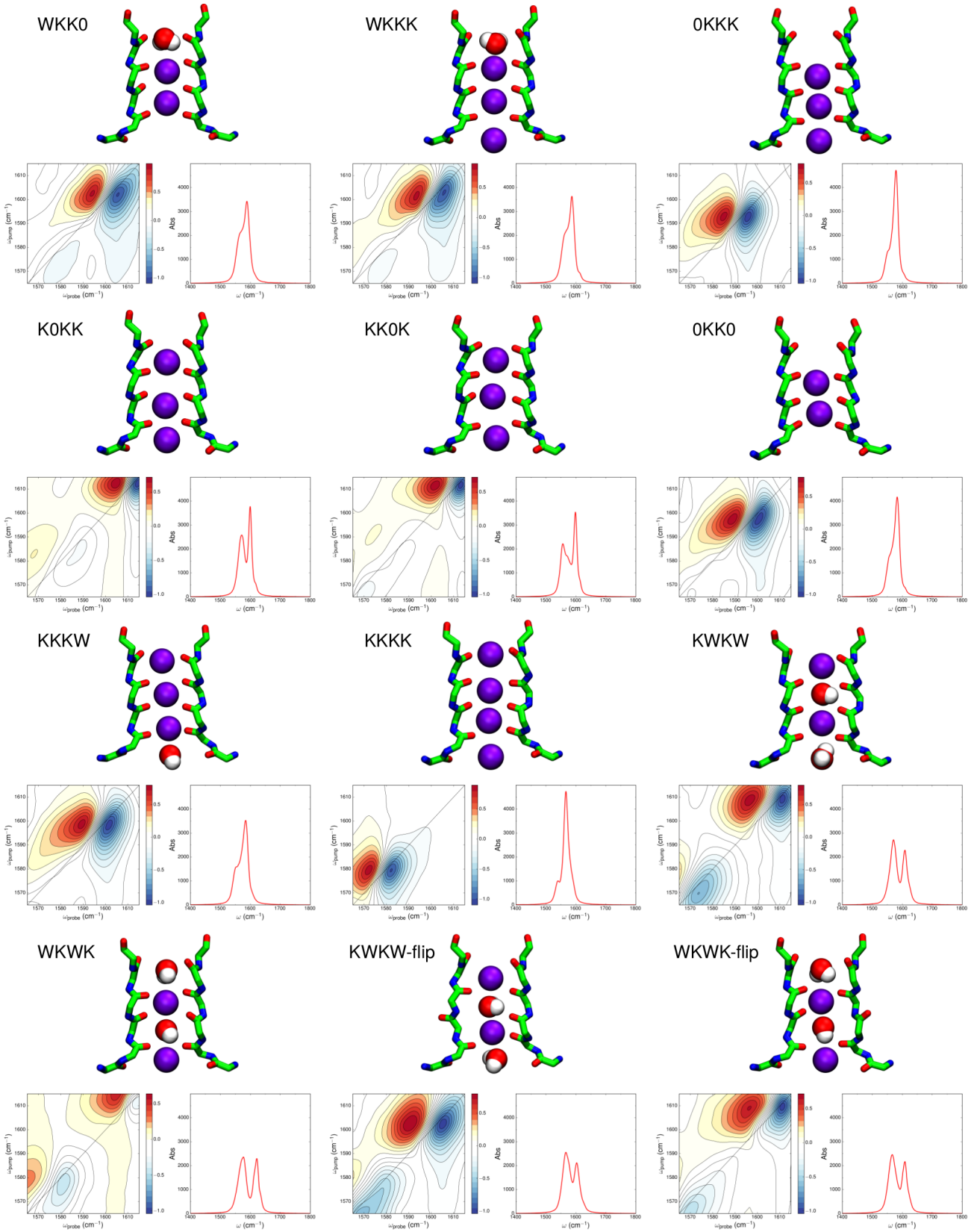
WKK0
WKKK
0KKK
K0KK
KK0K
0KK0
KKKW
KKKK
KWKW
WKWK
KWKW-flip
WKWK-flip
ω_pump (cm⁻¹)
ω_probe (cm⁻¹)
ω (cm⁻¹)
Abs

Supplementary Figure 5. Calculated IR spectra for individual SF occupancies considered in this work. Both 2D and 1D IR spectra are presented. In most of the states characteristic for the 'direct knock-on' mechanism, a single pair of peaks with high intensity is observed. Conversely, for states characteristic for the 'knock-on' mechanism, two pairs of peaks are observed. Considering 'direct knock-on' states, which are conductive in our simulations, a spectrum with two pairs of peaks seen in the experimental spectrum (Fig. 3 in the main text) is reproduced by the incorporation of WKK0 and KKKK states with high weights (40% and 25%, respectively). However, importantly, the final weight values were not extensively optimized. Note that we varied the weights only in 5% increments and that other weighting schemes can be found that lead to the same final conclusion.

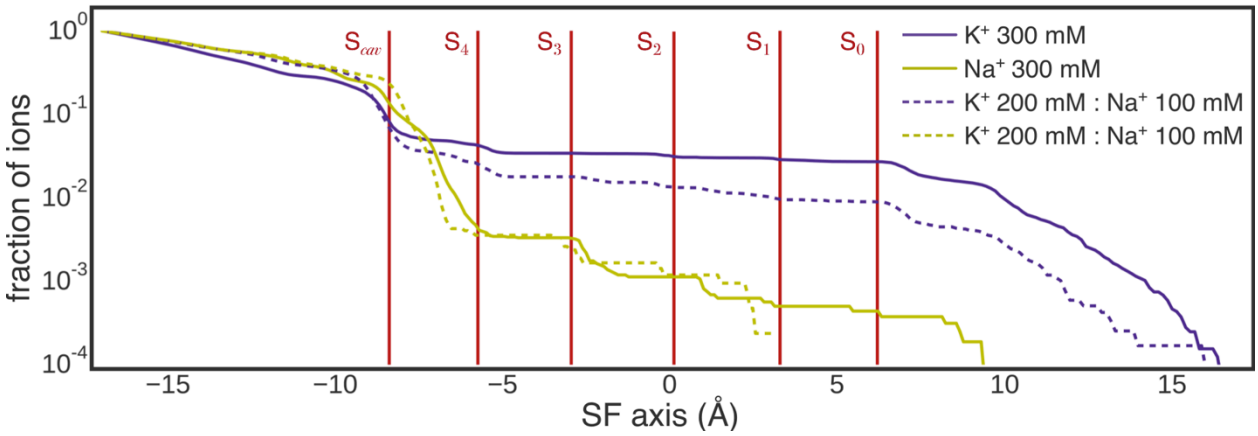

Supplementary Figure 6. Ionic reach in KcsA. The lines show the fraction of K^+ (purple lines) and Na^+ (yellow lines) ions that pass through the SF following their arrival from the channel cavity. Similar numbers of K^+ and Na^+ ions enter S_{cav}, initially, but only K^+ ions are able to cross the entire SF to a substantial degree.

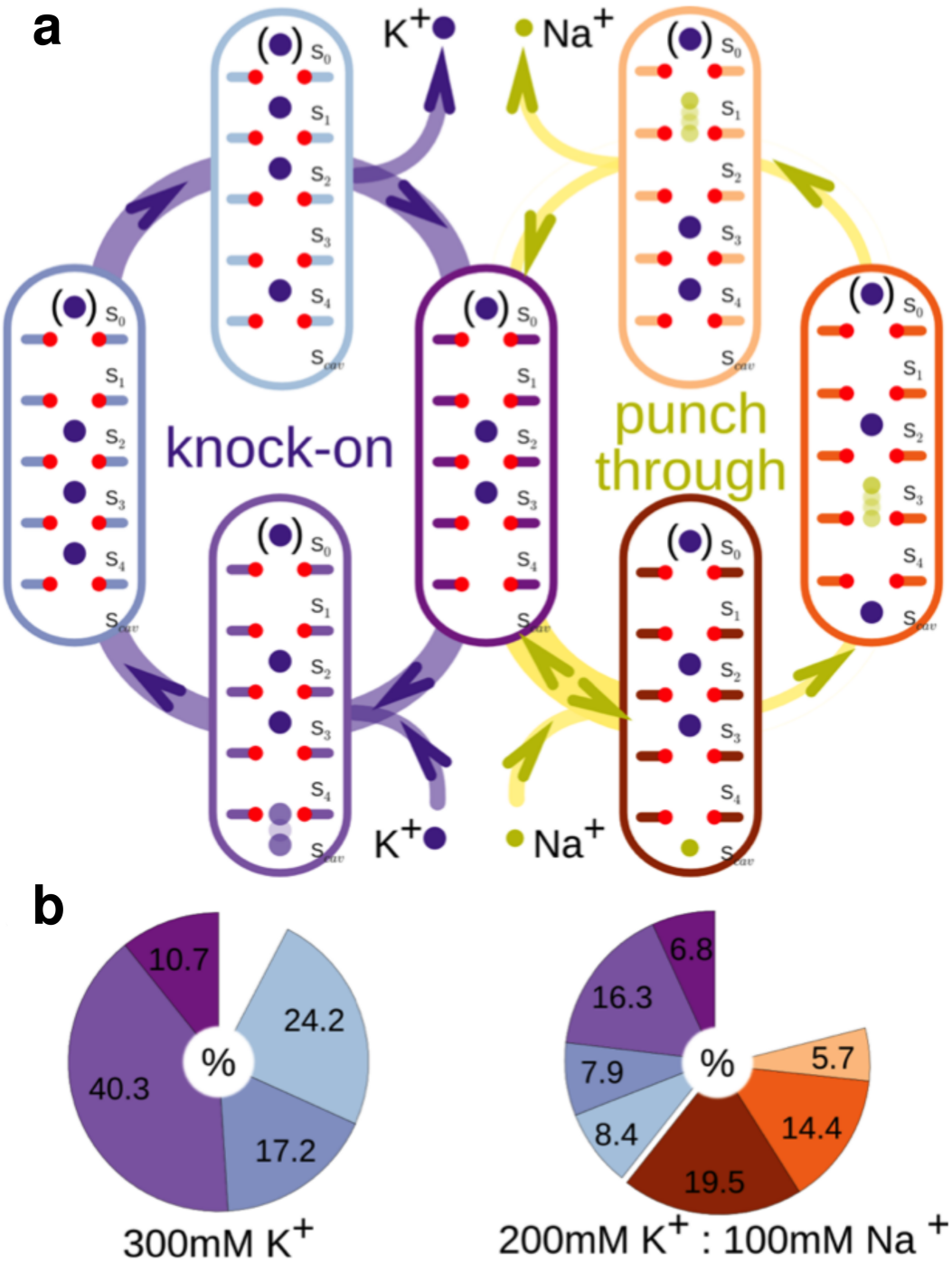
a
K+
Na+
knock-on
punch
through
K+
Na+
b
10.7
24.2
%
40.3
17.2
300mM K+
6.8
16.3
%
5.7
7.9
14.4
8.4
19.5
200mM K+ : 100mM Na +

Supplementary Figure 7. Most frequently encountered configurations of ions in the SF of KcsA. During permeation of K^+ (K^+ ions in purple, purple cycle on left) a K^+ ion entering from the cavity displaces the more tightly bound ions from S2 and S3 **(a)**. As Na^+ is introduced at high concentration, the most frequently found configuration corresponds to Na^+ block, with Na^+ reversibly bound to S_{cav} (Na^+ ions in yellow, yellow cycle on right). Very rarely, Na^+ ions are observed to enter the SF and to slowly transition through the channel. **(b)** Probability of specific ionic configurations in the SF for pure K^+ and K^+/Na^+ mixtures**.** Purple colours correspond to K^+ conductive ion configurations, brown or orange colors depict the internally (S_{cav}) Na^+ blocked situation (brown) and two stages of Na^+ ion "punch-through" which leads to slow Na^+ conduction.

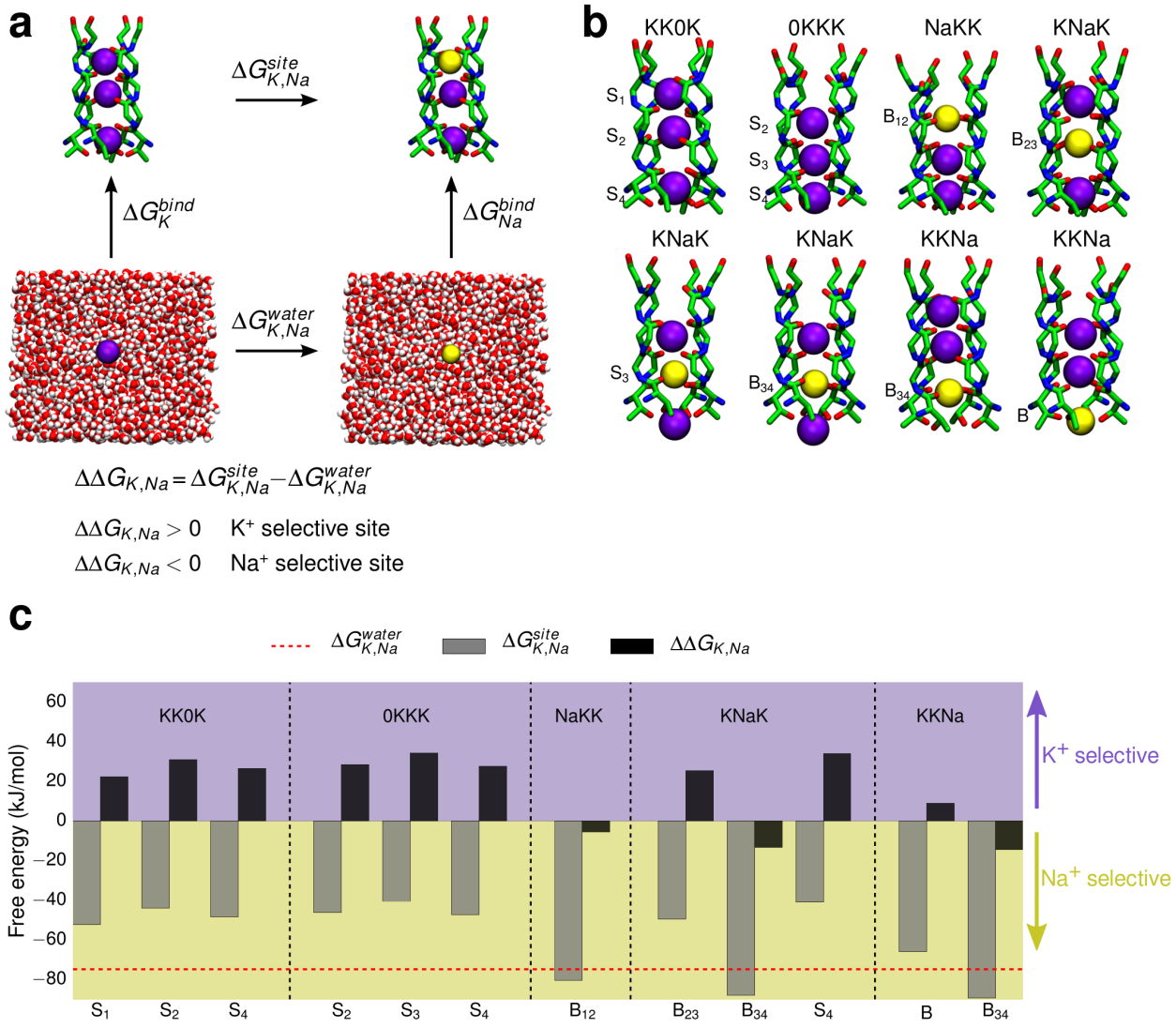

Supplementary Figure 8. Free energy calculations in KcsA. Potassium ions (purple spheres) are alchemically transformed into sodium ions (yellow spheres), and the associated free energy difference is computed. **(a)** Thermodynamic cycle for calculating the thermodynamic ion selectivity ($\Delta\Delta G_{K,Na}$), which is equal to the difference in free energies of transforming K^+ into Na^+ at a binding site ($\Delta G^{site}_{K,Na}$) compared to bulk water ($\Delta G^{water}_{K,Na}$, equal to 74.8 kJ/mol). By this definition, a given site is potassium-selective when $\Delta\Delta G_{K,Na} > 0$ and sodium-selective otherwise. Water is shown as red and white spheres, and the SF protein backbone as green licorice, with nitrogen atoms marked in blue and oxygen atoms in red. **(b)** Occupancy states with direct ion-ion contacts considered in the free energy calculations. The states were derived from computational electrophysiology simulations. Note that ions are not separated by water molecules. For the KK0K and 0KKK states, each potassium ion was transformed into a sodium ion. For the remaining states, a sodium ion was transformed into potassium. (**c**) Free energy values for both $\Delta G^{site}_{K,Na}$ and $\Delta\Delta G_{K,Na}$. Note that all canonical potassium binding sites S1-S4 are potassium selective due to the large dehydration penalty of sodium ions in the SF and only the B12 and B34 sites in-plane with the SF carbonyl groups are sodium selective.

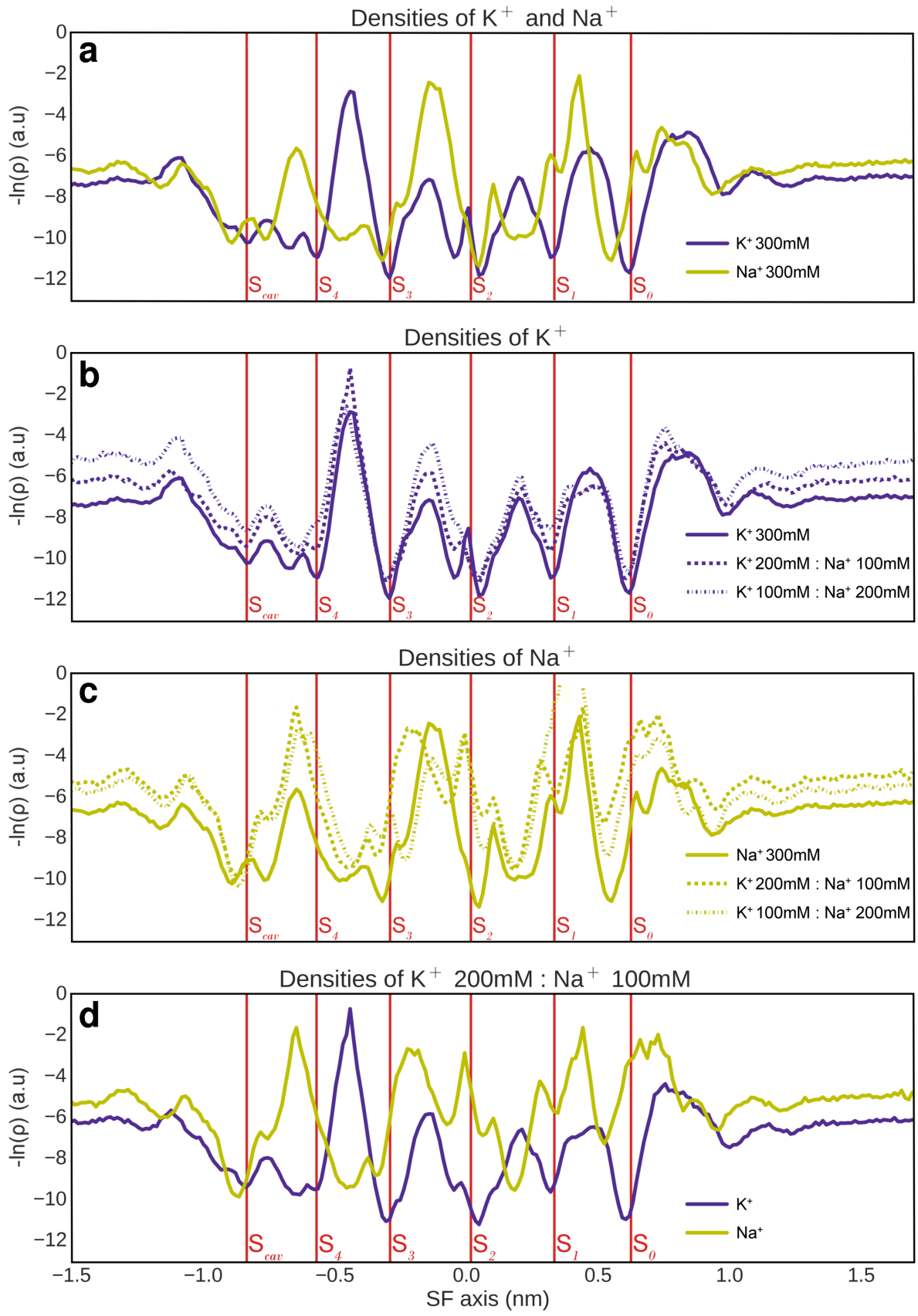
Densities of K+ and Na+
a
-ln(ρ) (a.u)
0
−2
−4
−6
−8
−10
−12
K+ 300mM
Na+ 300mM
Scav
S4
S3
S2
S1
S0
Densities of K+
b
-ln(ρ) (a.u)
K+ 300mM
K+ 200mM : Na+ 100mM
K+ 100mM : Na+ 200mM
Densities of Na+
c
-ln(ρ) (a.u)
Na+ 300mM
K+ 200mM : Na+ 100mM
K+ 100mM : Na+ 200mM
Densities of K+ 200mM : Na+ 100mM
d
-ln(ρ) (a.u)
K+
Na+
−1.5
−1.0
−0.5
0.0
0.5
1.0
1.5
SF axis (nm)

Supplementary Figure 9. Negative logarithmic densities for K^+ (purple lines) and Na^+ (yellow lines) ions inside the SF. The logarithmic ion densities represent quasi-free energies (with a nominal unit of k_bT). Density minima reflect stably bound ions (i.e. binding sites), while maxima indicate barriers between the binding sites. Vertical red lines mark the positions of the canonical potassium binding sites. **(a)** Densities in pure K^+ and Na^+ solutions. **(b)** Effect of Na^+ ions on potassium densities. **(c)** Effect of K^+ ions on sodium densities. **(d)** Densities in a mixed (200 mM K^+ and 100 mM Na^+) ionic solution. Note that some of the energy barriers for K^+ permeation increase in the presence of Na^+, owing to the binding of Na^+ to the in-plane sites.

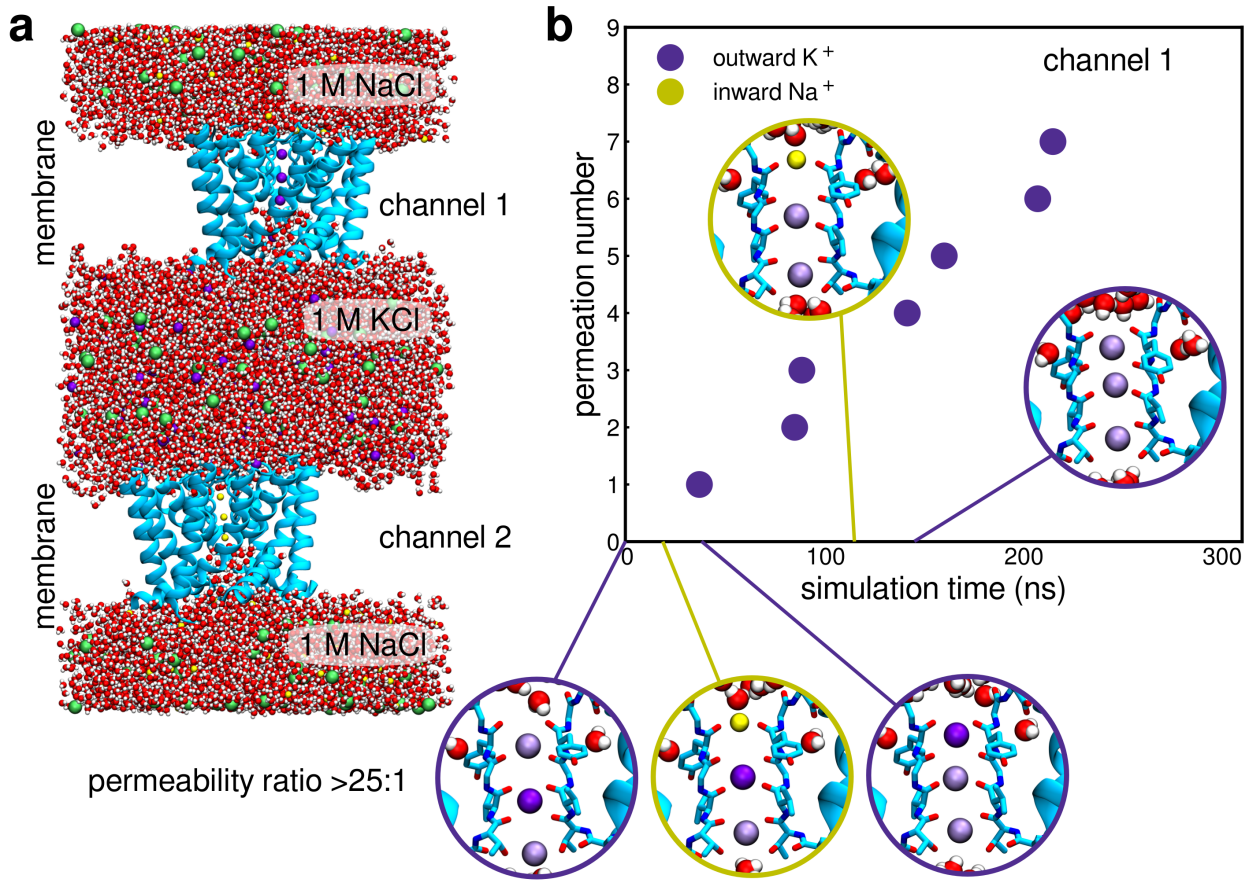

Supplementary Figure 10. Testing the selectivity for an outward K^+ and an inward Na^+ concentration gradient at 0 mV voltage. Under physiological conditions, K^+ ions flow from the intracellular to the extracellular side driven by a steep concentration gradient, while Na^+ ions are excluded from permeating inwards despite a Na^+ gradient of similar size in opposite direction. These conditions can be simulated by using a double membrane setup, with a KCl solution in one compartment, and NaCl solution in the other one **(a)**. The simulation shows strictly K^+ ion based outward permeation following the direct knock-on mechanism; Na^+ ions occasionally interact with the extracellular channel mouth but neither enter nor traverse the SF **(b)**.

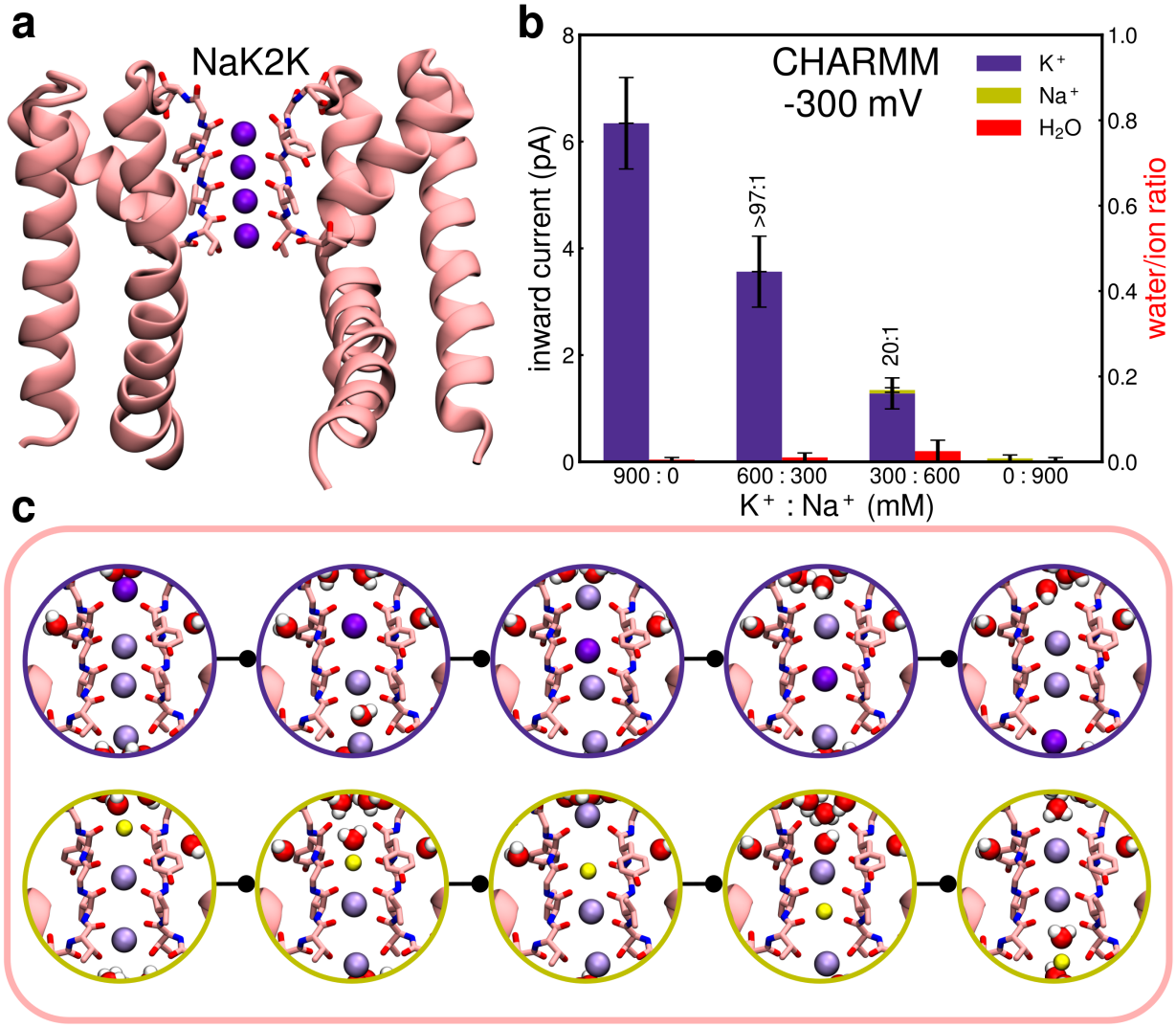

Supplementary Figure 11. Ion selectivity of NaK2K under a negative (hyperpolarised) membrane voltage. (a) Open state of the NaK2K channel. **(b)** Inward ion currents and water/ion permeation ratios at a voltage of ~-300 mV in pure solutions of K^+ or Na^+ as well as in mixed solutions. The inward currents observed are strongly K^+ selective, and water molecules are not seen to traverse the channel. **(c)** Ion permeation follows the direct knock-on mechanism, with the formation of ion pairs in adjacent ion binding sites.

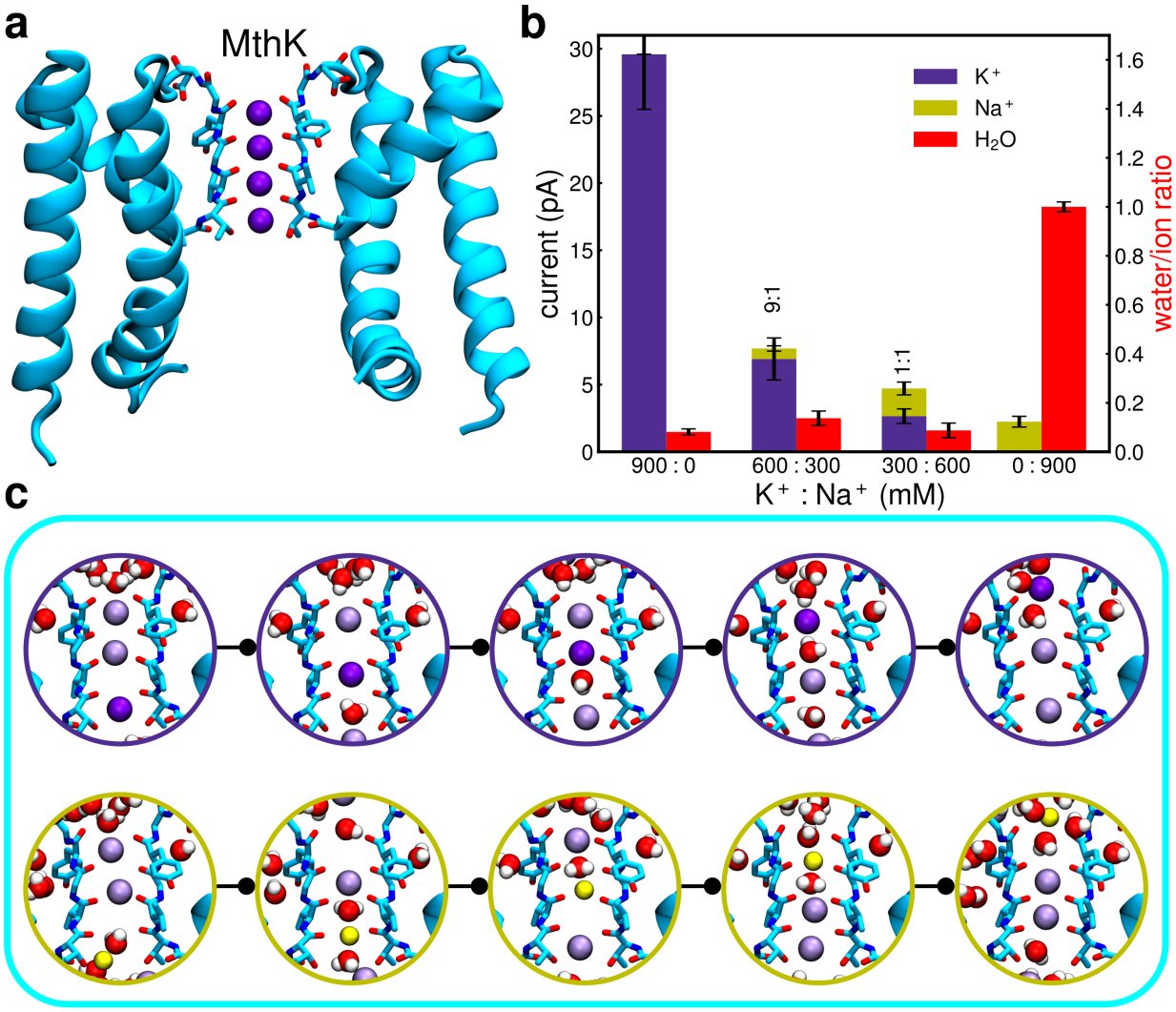

Supplementary Figure 12. Reduction in the ion selectivity of MthK under high positive voltage. (a) Open state of the MthK channel. **(b)** Ion currents and water/ion permeation ratios at a voltage of ~900 mV in pure solutions of K^+ or Na^+ as well as in mixed solutions. Applying high positive voltage increases the likelihood of water to be dragged along with ions permeating the SF **(c)**, leading to water/ion ratios of around 0.1 in mixed solutions. This, in turn, dramatically reduces the K^+/Na^+ selectivity of the channel. By contrast, MthK remains strictly impermeable to water molecules at 300 mV (see Fig. 2 in the main text).

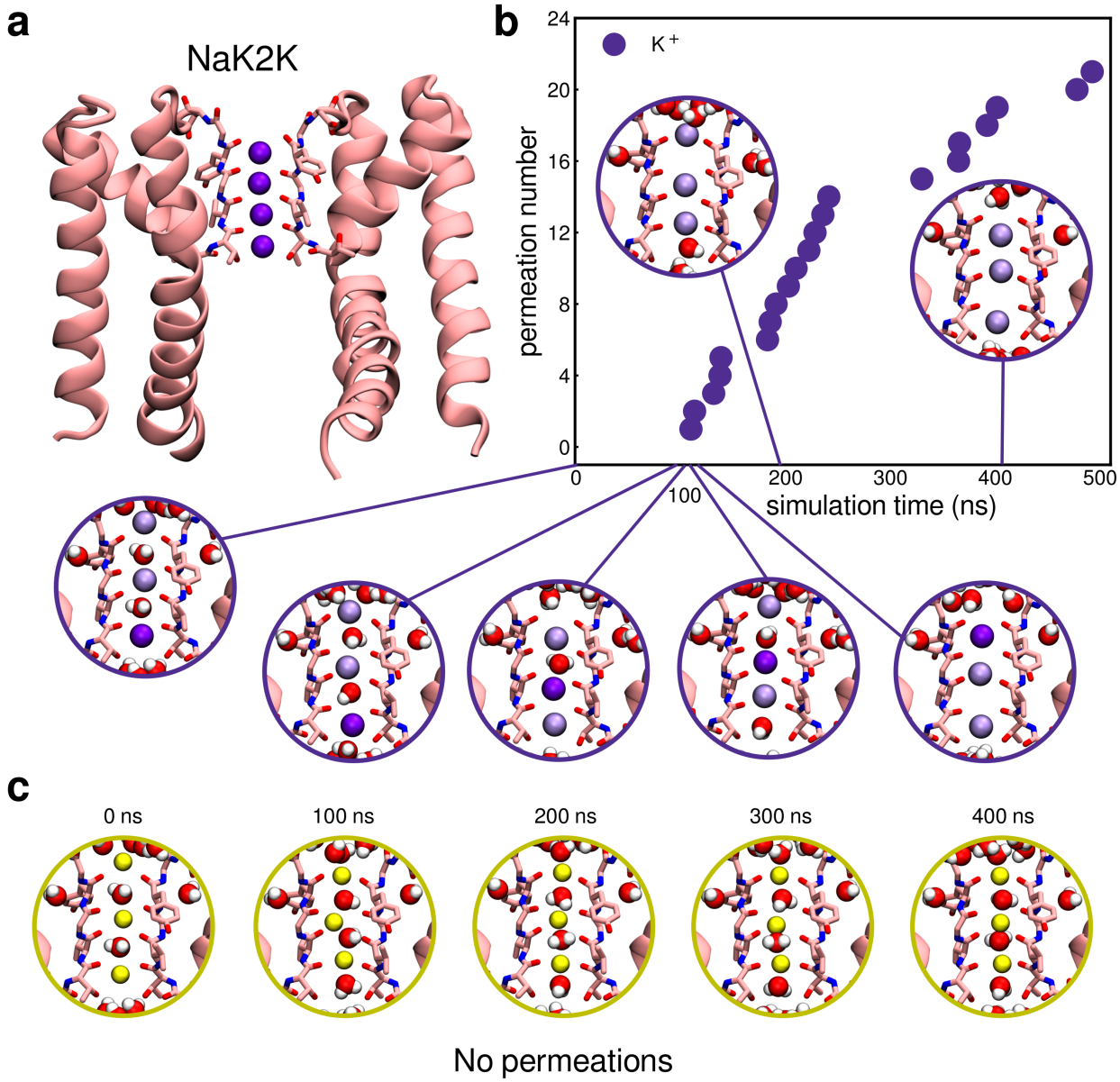

Supplementary Figure 13. Simulations of NaK2K initiated from water-containing configurations of the SF. (a) Open state of the NaK2K channel. **(b)** Time traces of K^+ ion permeation events in pure K^+ solutions, starting from a configuration of the SF containing water molecules located between K^+ ions (0 ns). For a time span of ~100 ns the channel remains non-conductive, until water molecules leave the SF. The subsequent ion permeation events follow the direct knock-on mechanism. In a pure Na^+ solution, by contrast, the channel remains non-conductive during the entire simulation **(c)**.

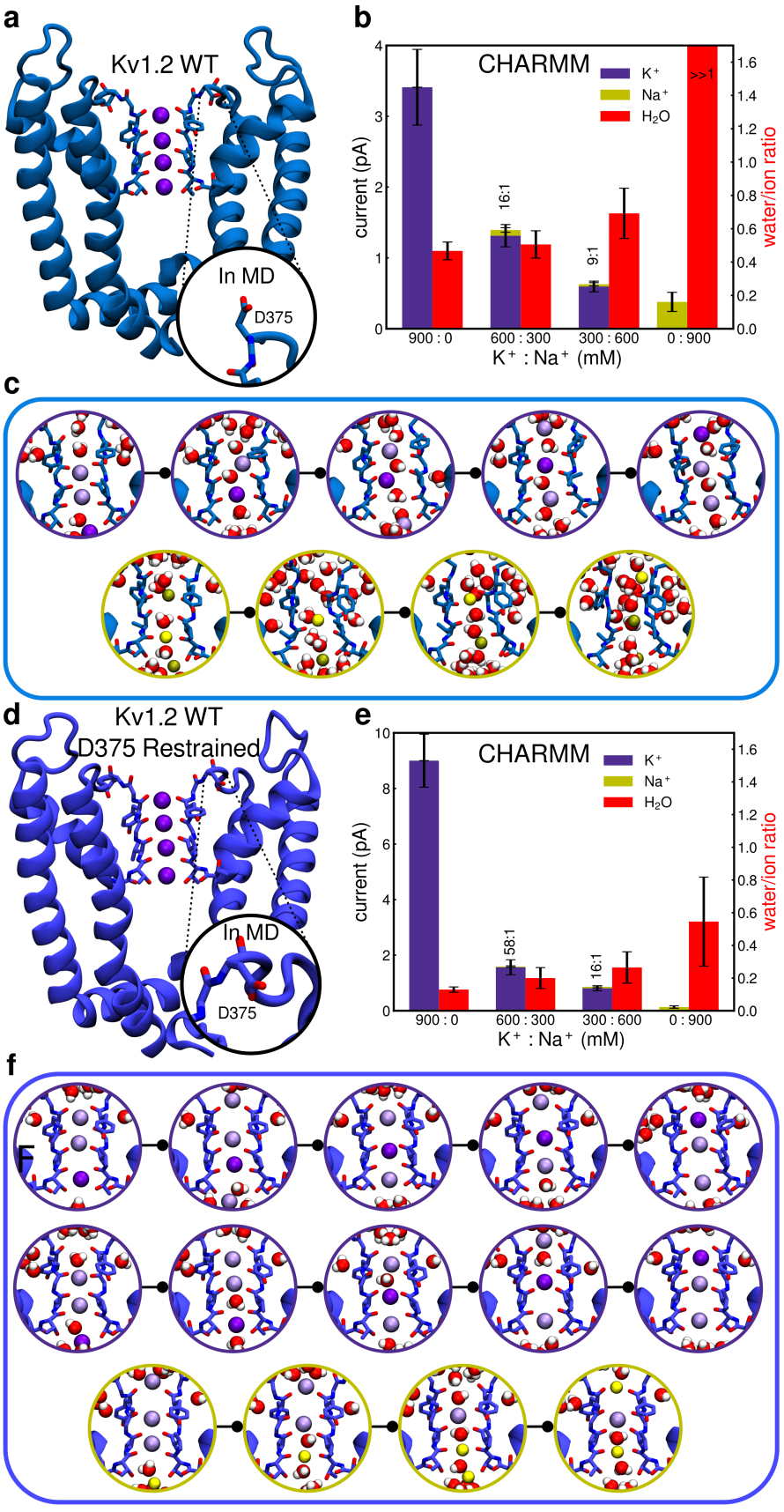
a
Kv1.2 WT
In MD
D375
b
CHARMM
K+
Na+
H2O
>>1
16:1
9:1
current (pA)
water/ion ratio
900 : 0
600 : 300
300 : 600
0 : 900
K+ : Na+ (mM)
c
d
Kv1.2 WT
D375 Restrained
In MD
D375
e
CHARMM
K+
Na+
H2O
58:1
16:1
current (pA)
water/ion ratio
900 : 0
600 : 300
300 : 600
0 : 900
K+ : Na+ (mM)
f
F

Supplementary Figure 14. Simulations of WT Kv1.2. (a) Crystal structure of the pore domain of the Kv1.2 channel (PDB id: 2r9r). The D375 residues near the extracellular exit of the SF are highlighted. In the crystal structure, the side chain of D375 is located within the protein, behind the SF, while in MD simulations it often flips towards the extracellular solution. **(b)** Ion currents and water/ion permeation ratios at a voltage of ~280 mV in pure solutions of K^+ or Na^+ as well as in mixed solutions. When D375 is flipped, the SF undergoes substantial overall distortion, which allows for more water co-permeation (~0.4 water/ion permeation ratio in pure K^+). This leads to a reduction in both the ionic currents and the ion selectivity of the channel. **(d, e)** When the D375 side-chain is restrained to its crystallographic position, the channel behaves similarly to the other K^+ selective channel types and the W362Y mutant reported in the main text (Fig. 2). **(c)** and **(f)** show typical simulation snapshots of ion permeation in the D375 flipped and non-flipped states, respectively.

4. Supplementary Tables

Supplementary Table 1. Details of KcsA MD simulations.

Channel **PDB**	**KcsA** **1k4c**			
Simulation setup	**Computational electrophysiology (~220 mV)**			
Simulation set	Pure K^+	2 : 1 K^+ : Na^+	1 : 2 K^+ : Na^+	Pure Na^+
Notes	F103 distance restrained, S6 helices restrained			
# waters	29052			
# ions	312 K^+	208 K^+ + 104 Na^+	104 K^+ + 208 Na^+	312 Na^+
# lipids	432			
Force field	**amber99sb with SPC/E, TIP3P or TIP4PEW water**			
Ions	Joung and Cheatham for a specific water model			
Lipids	Berger POPC			
Sampling				
Independent simulations	41	27	11	22
Total simulation time (ns)	35000	40000	20000	18000
Permeation events				
K^+	1206	503	124	0
Na^+	0	9	6	52
H_2O	1	14	4	12

Supplementary Table 2. Details of MthK MD simulations.

Channel PDB	**MthK 3ldc**			
Simulation setup	**Computational electrophysiology (~220 mV)**			
Simulation set	Pure K^+	2 : 1 K^+ : Na^+	1 : 2 K^+ : Na^+	Pure Na^+
Notes	-			
# waters	28273			
# ions	311 K^+	206 K^+ + 105 Na^+	105 K^+ + 206 Na^+	311 Na^+
# lipids	432			
Force field	**amber99sb with TIP3P water**			
Ions	Joung and Cheatham for TIP3P			
Lipids	Berger POPC			
Sampling				
Independent simulations	9	5	5	5
Total simulation time (ns)	9000	5000	5000	5000
Permeation events				
K^+	396	165	50	0
Na^+	0	0	0	0
H_2O	0	0	0	0

Supplementary Table 3. Details of NaK2K MD simulations.

Channel PDB	**NaK2K 3ouf**			
Simulation setup	**Applied electric field (~280 mV)**			
Simulation set	Pure K^+	2 : 1 K^+ : Na^+	1 : 2 K^+ : Na^+	Pure Na^+
Notes	-			
# waters	10300			
# ions	174 K^+	116 K^+ + 58 Na^+	58 K^+ + 116 Na^+	174 Na^+
# lipids	138			
Force field	**amber99sb with TIP3P water**			
Ions	Joung and Cheatham for TIP3P			
Lipids	Berger POPC			
Sampling				
Independent simulations	15	7	14	7
Total simulation time (ns)	6500	3500	7000	3500
Permeation events				
K^+	627	65	45	0
Na^+	0	0	0	3
H_2O	2	0	0	0

Supplementary Table 4. Details of control NaK2K MD simulations.

Channel PDB	**NaK2K 3ouf**			
Simulation setup	**Applied electric field (~280 mV)**			
Simulation set	Pure K^+	2 : 1 K^+ : Na^+	1 : 2 K^+ : Na^+	Pure Na^+
Notes	-			
# waters	10300			
# ions	174 K^+	116 K^+ + 58 Na^+	58 K^+ + 116 Na^+	174 Na^+
# lipids	138			
Force field	**CHARMM36 with CHARMM TIP3P water**			
Ions	CHARMM			
Lipids	CHARMM36 POPC			
Sampling				
Independent simulations	21	7	7	15
Total simulation time (ns)	10500	3500	3500	7500
Permeation events				
K^+	602	31	12	0
Na^+	0	1	0	0
H_2O	5	0	0	0

Supplementary Table 5. Details of Kv1.2 W362Y MD simulations.

Channel	**Kv1.2 W362Y**			
PDB	**2r9r**			
Simulation setup	**Applied electric field (~280 mV)**			
Simulation set	Pure K^+	2 : 1 K^+ : Na^+	1 : 2 K^+ : Na^+	Pure Na^+
Notes	W362Y stabilizing mutation introduced			
# waters	9989			
# ions	186 K^+	122 K^+ + 61 Na^+	61 K^+ + 122 Na^+	186 Na^+
# lipids	133			
Force field	**amber99sb*-ILDN with TIP3P water**			
Ions	Joung and Cheatham for TIP3P			
Lipids	Berger POPC			
Sampling				
Independent simulations	14	15	14	20
Total simulation time (ns)	7000	7500	7000	14000
Permeation events				
K^+	224	54	21	0
Na^+	0	0	0	0
H_2O	0	0	1	0

Supplementary Table 6. Details of control Kv1.2 W362Y MD simulations.

Channel PDB	**Kv1.2 W362Y 2r9r**			
Simulation setup	**Applied electric field (~280 mV)**			
Simulation set	Pure K^+	2 : 1 K^+ : Na^+	1 : 2 K^+ : Na^+	Pure Na^+
Notes	W362Y stabilizing mutation introduced			
# waters	9989			
# ions	186 K^+	122 K^+ + 61 Na^+	61 K^+ + 122 Na^+	186 Na^+
# lipids	133			
Force field	**CHARMM36 with CHARMM TIP3P water**			
Ions	CHARMM			
Lipids	CHARMM36 POPC			
Sampling				
Independent simulations	14	14	14	10
Total simulation time (ns)	7000	7000	7000	10000
Permeation events				
K^+	420	88	31	0
Na^+	0	2	1	0
H_2O	76	17	6	1

Supplementary Table 7. Details of Kv1.2 WT MD simulations.

Channel PDB	**Kv1.2 2r9r**			
Simulation setup	**Applied electric field (~280 mV)**			
Simulation set	Pure K^+	2 : 1 K^+ : Na^+	1 : 2 K^+ : Na^+	Pure Na^+
Notes	-			
# waters	9989			
# ions	186 K^+	122 K^+ + 61 Na^+	61 K^+ + 122 Na^+	186 Na^+
# lipids	133			
Force field	**CHARMM36 with CHARMM TIP3P water**			
Ions	CHARMM			
Lipids	CHARMM36 POPC			
Sampling				
Independent simulations	16	20	20	11
Total simulation time (ns)	8000	10000	10000	5500
Permeation events				
K^+	182	82	37	0
Na^+	0	5	2	13
H_2O	85	44	27	>100

Supplementary Table 8. Details of Kv1.2 WT D375 restrained MD simulations.

Channel PDB	**Kv1.2 2r9r**			
Simulation setup	**Applied electric field (~280 mV)**			
Simulation set	Pure K^+	2 : 1 K^+ : Na^+	1 : 2 K^+ : Na^+	Pure Na^+
Notes	Side-chains of D375 restrained			
# waters	9989			
# ions	186 K^+	122 K^+ + 61 Na^+	61 K^+ + 122 Na^+	186 Na^+
# lipids	133			
Force field	**CHARMM36 with CHARMM TIP3P water**			
Ions	CHARMM			
Lipids	CHARMM36 POPC			
Sampling				
Independent simulations	15	11	13	11
Total simulation time (ns)	7500	5500	6500	5500
Permeation events				
K^+	510	54	32	0
Na^+	0	1	2	6
H_2O	66	11	9	11

Supplementary Table 9. Details of NaK2CNG-N MD simulations.

Channel	**NaK2CNG-N**			
PDB	**3k06**			
Simulation setup	**Applied electric field (~280 mV)**			
Simulation set	Pure K^+	2 : 1 K^+ : Na^+	1 : 2 K^+ : Na^+	Pure Na^+
Notes	-			
# waters	10385			
# ions	171 K^+	114 K^+ + 57 Na^+	57 K^+ + 114 Na^+	171 Na^+
# lipids	139			
Force field	**amber99sb with TIP3P water**			
Ions	Joung and Cheatham for TIP3P			
Lipids	Berger POPC			
Sampling				
Independent simulations	30	36	45	42
Total simulation time (ns)	15000	18000	22500	21000
Permeation events				
K^+	152	221	119	0
Na^+	0	57	69	116
H_2O	>500	>500	>500	>500

Supplementary Table 10. List of SF occupancies considered in spectral calculations. The letters denote the occupancy of the sites S1 to S4 (from left to right), with 'K' representing a K^+ ion, 'W' a water molecule and '0' a vacancy. Note that in some cases K^+ ions can be additionally bound to S0 and/or Scav, however this does not appreciably affect the final spectrum.

Spectral calculations (KcsA)

Occupancy	Notes
'direct knock-on'	
KKKK	
0KKK	K^+ ion often bound to S0
K0KK	K^+ ion often bound to S0
KK0K	
0KK0	K^+ ion often bound to S0 and Scav
WKK0	
WKKK	
KKKW	
'knock-on'	
KWKW	
WKWK	K^+ ion often bound to S0
KWKW-flipped	One Val76 flipped
WKWK-flipped	One Val76 flipped

Supplementary Table 11. Free energy differences between K^+ and Na^+ ions at the specific ion binding sites in the SF filter of KcsA ($\Delta G^{site}_{K,Na}$) and the overall thermodynamic selectivity ($\Delta\Delta G_{K,Na}$) at these sites. The negative value of $\Delta\Delta G_{K,Na}$ means the site is selective for K^+ ions. See Figure S8 the definition of the binding sites.

Free energy calculations (KcsA)

Site	$\Delta G^{site}_{K,Na}$ (kJ/mol)	$\Delta\Delta G_{K,Na}$(kJ/mol)
Occupancy KK0K		
S_1	-52.3 (0.6)	-22.5 (0.6)
S_2	-43.9 (0.4)	-30.9 (0.4)
S_4	-48.3 (0.3)	-26.5 (0.5)
Occupancy 0KKK		
S_2	-46.2 (0.6)	-28.6 (0.6)
S_3	-40.5 (1.0)	-34.3 (1.1)
S_4	-47.2 (0.7)	-27.6 (0.8)
Occupancy NaKK		
B_{12}	-80.4 (0.1)	+5.6 (0.2)
Occupancy KNaK		
B_{23}	-49.6 (0.5)	-25.3 (0.6)
S_3	-40.8 (0.7)	-34.0 (0.8)
B_{34}	-88.0 (0.6)	+13.2 (0.7)
Occupancy KKNa		
B_{34}	-89.3 (0.4)	+14.5 (0.5)
B	-65.8 (0.4)	-9.0 (0.5)

5. References

1 Kutzner, C., Grubmuller, H., de Groot, B. L. & Zachariae, U. Computational electrophysiology: the molecular dynamics of ion channel permeation and selectivity in atomistic detail. *Biophys. J.* **101**, 809-817 (2011).

2 Kutzner, C. *et al.* Insights into the function of ion channels by computational electrophysiology simulations. *Biochim. Biophys. Acta* **1858**, 1741-1752 (2016).

3 Cuello, L. G., Jogini, V., Cortes, D. M. & Perozo, E. Structural mechanism of C-type inactivation in K(+) channels. *Nature* **466**, 203-208 (2010).

4 Zhou, Y., Morais-Cabral, J. H., Kaufman, A. & MacKinnon, R. Chemistry of ion coordination and hydration revealed by a K+ channel-Fab complex at 2.0 A resolution. *Nature* **414**, 43-48 (2001).

5 Kopfer, D. A. *et al.* Ion permeation in K(+) channels occurs by direct Coulomb knock-on. *Science* **346**, 352-355 (2014).

6 Ye, S., Li, Y. & Jiang, Y. Novel insights into K+ selectivity from high-resolution structures of an open K+ channel pore. *Nat Struct Mol Biol* **17**, 1019-1023 (2010).

7 Bhate, M. P. & McDermott, A. E. Protonation state of E71 in KcsA and its role for channel collapse and inactivation. *Proc. Natl. Acad. Sci. U. S. A* **109**, 15265-15270 (2012).

8 Van Der Spoel, D. *et al.* GROMACS: fast, flexible, and free. *J. Comput. Chem.* **26**, 1701-1718 (2005).

9 Hess, B., Kutzner, C., van der Spoel, D. & Lindahl, E. GROMACS 4: Algorithms for Highly Efficient, Load-Balanced, and Scalable Molecular Simulation. *J. Chem. Theory Comput.* **4**, 435-447 (2008).

10 Pronk, S. *et al.* GROMACS 4.5: a high-throughput and highly parallel open source molecular simulation toolkit. *Bioinformatics* **29**, 845-854 (2013).

11 Abraham, M. J. *et al.* GROMACS: High performance molecular simulations through multi-level parallelism from laptops to supercomputers. *SoftwareX* **1–2**, 19-25 (2015).

12 Hornak, V. *et al.* Comparison of multiple Amber force fields and development of improved protein backbone parameters. *Proteins* **65**, 712-725 (2006).

13 Berendsen, H. J. C., Grigera, J. R. & Straatsma, T. P. The missing term in effective pair potentials. *J. Phys. Chem.* **91**, 6269-6271 (1987).

14 Jorgensen, W. L., Chandrasekhar, J., Madura, J. D., Impey, R. W. & Klein, M. L. Comparison of simple potential functions for simulating liquid water. *J. Chem. Phys.* **79**, 926-935 (1983).

15 Horn, H. W. *et al.* Development of an improved four-site water model for biomolecular simulations: TIP4P-Ew. *J. Chem. Phys.* **120**, 9665-9678 (2004).

16 Joung, I. S. & Cheatham, T. E., 3rd. Determination of alkali and halide monovalent ion parameters for use in explicitly solvated biomolecular simulations. *J. Phys. Chem. B* **112**, 9020-9041 (2008).

17 Berger, O., Edholm, O. & Jahnig, F. Molecular dynamics simulations of a fluid bilayer of dipalmitoylphosphatidylcholine at full hydration, constant pressure, and constant temperature. *Biophys. J.* **72**, 2002-2013 (1997).

18 Bachar, M., Brunelle, P., Tieleman, D. P. & Rauk, A. Molecular Dynamics Simulation of a Polyunsaturated Lipid Bilayer Susceptible to Lipid Peroxidation. *J. Phys. Chem. B* **108**, 7170-7179 (2004).
19 Cordomi, A., Caltabiano, G. & Pardo, L. Membrane Protein Simulations Using AMBER Force Field and Berger Lipid Parameters. *J. Chem. Theory Comput.* **8**, 948-958 (2012).
20 Feenstra, K. A., Hess, B. & Berendsen, H. J. C. Improving efficiency of large time-scale molecular dynamics simulations of hydrogen-rich systems. *J. Comput. Chem.* **20**, 786-798 (1999).
21 Bjelkmar, P., Larsson, P., Cuendet, M. A., Hess, B. & Lindahl, E. Implementation of the CHARMM Force Field in GROMACS: Analysis of Protein Stability Effects from Correction Maps, Virtual Interaction Sites, and Water Models. *J. Chem. Theory Comput.* **6**, 459-466 (2010).
22 Hess, B., Bekker, H., Berendsen, H. J. C. & Fraaije, J. G. E. M. LINCS: A linear constraint solver for molecular simulations. *J. Comput. Chem.* **18**, 1463-1472 (1997).
23 Verlet, L. Computer "Experiments" on Classical Fluids. I. Thermodynamical Properties of Lennard-Jones Molecules. *Phys. Rev.* **159**, 98-103 (1967).
24 Darden, T., York, D. & Pedersen, L. Particle mesh Ewald: An N·log(N) method for Ewald sums in large systems. *J. Chem. Phys.* **98**, 10089-10092 (1993).
25 Bussi, G., Donadio, D. & Parrinello, M. Canonical sampling through velocity rescaling. *J. Chem. Phys.* **126**, 014101 (2007).
26 Berendsen, H. J. C., Postma, J. P. M., van Gunsteren, W. F., DiNola, A. & Haak, J. R. Molecular dynamics with coupling to an external bath. *J. Chem. Phys.* **81**, 3684-3690 (1984).
27 Long, S. B., Tao, X., Campbell, E. B. & MacKinnon, R. Atomic structure of a voltage-dependent K+ channel in a lipid membrane-like environment. *Nature* **450**, 376-382 (2007).
28 Jensen, M. O. *et al.* Principles of conduction and hydrophobic gating in K+ channels. *Proc. Natl. Acad. Sci. U.S.A* **107**, 5833-5838 (2010).
29 Sauer, D. B., Zeng, W., Raghunathan, S. & Jiang, Y. Protein interactions central to stabilizing the K+ channel selectivity filter in a four-sited configuration for selective K+ permeation. *Proc. Natl. Acad. Sci. U.S.A* **108**, 16634-16639 (2011).
30 Jo, S., Kim, T., Iyer, V. G. & Im, W. CHARMM-GUI: a web-based graphical user interface for CHARMM. *J. Comput. Chem.* **29**, 1859-1865 (2008).
31 Jo, S., Kim, T. & Im, W. Automated builder and database of protein/membrane complexes for molecular dynamics simulations. *PLoS One* **2**, e880 (2007).
32 Jo, S., Lim, J. B., Klauda, J. B. & Im, W. CHARMM-GUI Membrane Builder for mixed bilayers and its application to yeast membranes. *Biophys. J.* **97**, 50-58 (2009).
33 Wu, E. L. *et al.* CHARMM-GUI Membrane Builder toward realistic biological membrane simulations. *J. Comput. Chem.* **35**, 1997-2004 (2014).
34 Lee, J. *et al.* CHARMM-GUI Input Generator for NAMD, GROMACS, AMBER, OpenMM, and CHARMM/OpenMM Simulations Using the CHARMM36 Additive Force Field. *J. Chem. Theory. Comput.* **12**, 405-413 (2016).
35 Best, R. B. & Hummer, G. Optimized molecular dynamics force fields applied to the helix-coil transition of polypeptides. *J. Phys. Chem. B* **113**, 9004-9015 (2009).
36 Derebe, M. G. *et al.* Tuning the ion selectivity of tetrameric cation channels by changing the number of ion binding sites. *Proc. Natl. Acad. Sci. U.S.A* **108**, 598-602 (2011).

37 Derebe, M. G., Zeng, W., Li, Y., Alam, A. & Jiang, Y. Structural studies of ion permeation and Ca2+ blockage of a bacterial channel mimicking the cyclic nucleotide-gated channel pore. *Proc. Natl. Acad. Sci. U.S.A* **108**, 592-597 (2011).
38 Sauer, D. B., Zeng, W., Canty, J., Lam, Y. & Jiang, Y. Sodium and potassium competition in potassium-selective and non-selective channels. *Nat. Commun.* **4**, 2721 (2013).
39 Roux, B. The membrane potential and its representation by a constant electric field in computer simulations. *Biophys. J.* **95**, 4205-4216 (2008).
40 Gumbart, J., Khalili-Araghi, F., Sotomayor, M. & Roux, B. Constant electric field simulations of the membrane potential illustrated with simple systems. *Biochim. Biophys. Acta* **1818**, 294-302 (2012).
41 Lindorff-Larsen, K. *et al.* Improved side-chain torsion potentials for the Amber ff99SB protein force field. *Proteins* **78**, 1950-1958 (2010).
42 Best, R. B. *et al.* Optimization of the additive CHARMM all-atom protein force field targeting improved sampling of the backbone phi, psi and side-chain chi(1) and chi(2) dihedral angles. *J. Chem. Theory Comput.* **8**, 3257-3273 (2012).
43 Klauda, J. B. *et al.* Update of the CHARMM all-atom additive force field for lipids: validation on six lipid types. *J. Phys. Chem. B* **114**, 7830-7843 (2010).
44 Huang, J. *et al.* CHARMM36m: an improved force field for folded and intrinsically disordered proteins. *Nat. Methods* **14**, 71-73 (2017).
45 Beglov, D. & Roux, B. Finite representation of an infinite bulk system: Solvent boundary potential for computer simulations. *J. Chem. Phys.* **100**, 9050-9063 (1994).
46 Jensen, M. O., Jogini, V., Eastwood, M. P. & Shaw, D. E. Atomic-level simulation of current-voltage relationships in single-file ion channels. *J. Gen. Physiol.* **141**, 619-632 (2013).
47 Hoover, W. G. Canonical dynamics: Equilibrium phase-space distributions. *Phys. Rev. A* **31**, 1695-1697 (1985).
48 Nosé, S. A unified formulation of the constant temperature molecular dynamics methods. *J. Chem. Phys.* **81**, 511-519 (1984).
49 Parrinello, M. & Rahman, A. Polymorphic transitions in single crystals: A new molecular dynamics method. *J. Appl. Phys.* **52**, 7182-7190 (1981).
50 Kratochvil, H. T. *et al.* Instantaneous ion configurations in the K+ ion channel selectivity filter revealed by 2D IR spectroscopy. *Science* **353**, 1040-1044 (2016).
51 Berneche, S. & Roux, B. Energetics of ion conduction through the K+ channel. *Nature* **414**, 73-77 (2001).
52 Jansen, T. & Knoester, J. Nonadiabatic effects in the two-dimensional infrared spectra of peptides: application to alanine dipeptide. *J. Phys. Chem. B* **110**, 22910-22916 (2006).
53 Liang, C. & Jansen, T. L. An Efficient N(3)-Scaling Propagation Scheme for Simulating Two-Dimensional Infrared and Visible Spectra. *J. Chem. Theory Comput.* **8**, 1706-1713 (2012).
54 Wang, L., Middleton, C. T., Zanni, M. T. & Skinner, J. L. Development and validation of transferable amide I vibrational frequency maps for peptides. *J. Phys. Chem. B* **115**, 3713-3724 (2011).
55 Cunha, A. V., Bondarenko, A. S. & Jansen, T. L. Assessing Spectral Simulation Protocols for the Amide I Band of Proteins. *J. Chem. Theory Comput.* **12**, 3982-3992 (2016).

56 Bondarenko, A. S. & Jansen, T. L. Application of two-dimensional infrared spectroscopy to benchmark models for the amide I band of proteins. *J. Chem. Phys.* **142**, 212437 (2015).
57 Jansen, T. l. C., Dijkstra, A. G., Watson, T. M., Hirst, J. D. & Knoester, J. Modeling the amide I bands of small peptides. *J. Chem. Phys.* **125**, 044312 (2006).
58 Torii, H. & Tasumi, M. Ab initio molecular orbital study of the amide I vibrational interactions between the peptide groups in di- and tripeptides and considerations on the conformation of the extended helix. *J. Raman Spectrosc.* **29**, 81-86 (1998).
59 Marcus, Y. A simple empirical model describing the thermodynamics of hydration of ions of widely varying charges, sizes, and shapes. *Biophys. Chem.* **51**, 111-127 (1994).
60 Tissandier, M. D. *et al.* The Proton's Absolute Aqueous Enthalpy and Gibbs Free Energy of Solvation from Cluster-Ion Solvation Data. *J. Phys. Chem. A* **102**, 7787-7794 (1998).
61 Thompson, A. N. *et al.* Mechanism of potassium-channel selectivity revealed by Na(+) and Li(+) binding sites within the KcsA pore. *Nat. Struct. Mol. Biol.* **16**, 1317-1324 (2009).
62 Kim, I. & Allen, T. W. On the selective ion binding hypothesis for potassium channels. *Proc. Natl. Acad. Sci. U.S.A* **108**, 17963-17968 (2011).
63 Shirts, M. R. & Chodera, J. D. Statistically optimal analysis of samples from multiple equilibrium states. *J. Chem. Phys.* **129**, 124105 (2008).
64 Klimovich, P. V., Shirts, M. R. & Mobley, D. L. Guidelines for the analysis of free energy calculations. *J. Comput. Aided Mol. Des.* **29**, 397-411 (2015).
65 Andersen, O. S. Perspectives on: Ion selectivity. *J. Gen. Physiol.* **137**, 393-395 (2011).
66 Eisenman, G. Cation Selective Glass Electrodes and their Mode of Operation. *Biophys. J.* **2**, 259-323 (1962).
67 Lockless, S. W. Structural and Thermodynamic Properties of Selective Ion Binding in a K(+) Channel. *PLoS Biol.* **5** (2007).
68 Thomas, M., Jayatilaka, D. & Corry, B. The predominant role of coordination number in potassium channel selectivity. *Biophys. J.* **93**, 2635-2643 (2007).
69 Schmid, R., Miah, A. M. & Sapunov, V. N. A new table of the thermodynamic quantities of ionic hydration: values and some applications (enthalpy-entropy compensation and Born radii). *Phys. Chem. Chem. Phys.* **2**, 97-102 (2000).
70 Neyton, J. & Miller, C. Discrete Ba2+ block as a probe of ion occupancy and pore structure in the high-conductance Ca2+ -activated K+ channel. *J. Gen. Physiol.* **92**, 569-586 (1988).
71 Armstrong, C. M. & Taylor, S. R. Interaction of barium ions with potassium channels in squid giant axons. *Biophys. J.* **30**, 473-488 (1980).
72 Eaton, D. C. & Brodwick, M. S. Effects of barium on the potassium conductance of squid axon. *J. Gen. Physiol.* **75**, 727-750 (1980).